ACS APPLIED MATERIALS & INTERFACES

Research Article

www.acsami.org

Target-Catalyzed DNA Four-Way Junctions for CRET Imaging of MicroRNA, Concatenated Logic Operations, and Self-Assembly of DNA Nanohydrogels for Targeted Drug Delivery

Sai Bi,*[,†,‡] Bao Xiu,[§] Jiayan Ye,[§] and Ying Dong[§]

[†]Shandong Province Key Laboratory of Detection Technology for Tumor Markers, School of Chemistry and Chemical Engineering, Linyi University, Linyi 276005, China

[‡]Collaborative Innovation Center for Marine Biomass Fiber Materials and Textiles, College of Chemical Science and Engineering, Laboratory of Fiber Materials and Modern Textiles, the Growing Base for State Key Laboratory, Shandong Sino-Japanese Center for Collaborative Research of Carbon Nanomaterials, Qingdao University, Qingdao 266071, China

[§]Key Laboratory of Sensor Analysis of Tumor Marker, Ministry of Education, College of Chemistry and Molecular Engineering, Qingdao University of Science and Technology, Qingdao 266042, China

Supporting Information

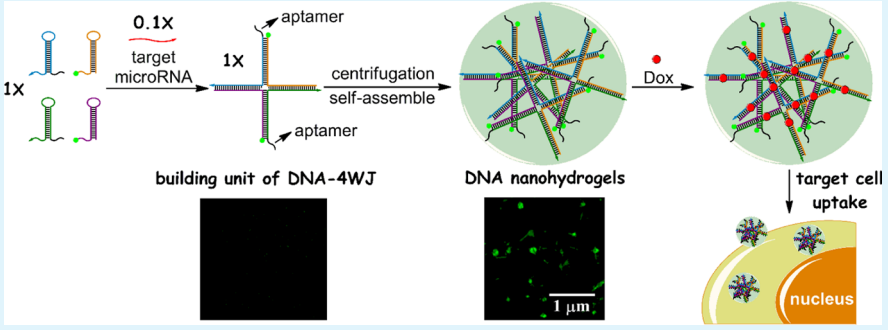

ABSTRACT: Here we report a target-catalyzed DNA four-way junction (DNA-4WJ) on the basis of toehold-mediated DNA strand displacement reaction (TM-SDR), which is readily applied in enzyme-free amplified chemiluminescence resonance energy transfer (CRET) imaging of microRNA. In this system, the introduction of target microRNA-let-7a (miR-let-7a) activates a cascade of assembly steps with four DNA hairpins, followed by a disassembly step in which the target microRNA is displaced and released from DNA-4WJ to catalyze the self-assembly of additional branched junctions. As a result, G-quadruplex subunit sequences and fluorophore fluorescein amidite (FAM) are encoded in DNA-4WJ in a close proximity, stimulating a CRET process in the presence of hemin/K^+ to form horseradish peroxidase (HRP)-mimicking DNAzyme that catalyzes the generation of luminol/H_2O_2 chemiluminescence (CL), which further transfers to FAM. The background signal is easily reduced using magnetic graphene oxide (MGO) to remove unreacted species through magnetic separation, which makes a great contribution to improve the detection sensitivity and achieves a detection limit as low as 6.9 fM microRNA-let-7a (miR-let-7a). In addition, four-input concatenated logic circuits with an automatic reset function have been successfully constructed relying on the architecture of the proposed DNA-4WJ. More importantly, DNA nanohydrogels are self-assembled using DNA-4WJs as building units after centrifugation, which are driven by liquid crystallization and dense packaging of building units. Moreover, the DNA nanohydrogels are readily functionalized by incorporating with aptamers, bioimaging agents, and drug loading sites, which thus are served as efficient nanocarriers for targeted drug delivery and cancer therapy with high loading capacity and excellent biocompatibility.

KEYWORDS: *toehold-mediated strand displacement, DNA four-way junction, concatenated logic circuits, DNA nanohydrogels, targeted drug delivery*

INTRODUCTION

Nucleic acid nanotechnology has emerged as a popular tool for versatile applications, such as development of biosensing and biocomputing platforms,[1,2] assembly of nanostructures,[3] and biomedical and biotechnological applications.[4] Owing to the exquisite recognition properties encoded in the specific interaction of Watson−Crick base-pairing, DNA toehold-mediated strand-displacement reactions (TM-SDR) have attracted ever-increasing interest in amplifying the recognition events.[5] In a typical DNA TM-SDR process, one short DNA

Received: August 24, 2015
Accepted: September 30, 2015
Published: September 30, 2015

DOI: 10.1021/acsami.5b07827
ACS Appl. Mater. Interfaces 2015, 7, 23310−23319

strand hybridizes with a portion of a long DNA, leaving an exposed single-stranded domain (termed as "toehold"). The short DNA can be displaced by an auxiliary DNA strand that contains the complementary sequence to the "toehold" domain and more complementary base pairs to long DNA strand, resulting in the formation of a new DNA duplex structure with enhanced stability.[6] So far, TM-SDR has been widely explored in the field of amplified sensing,[7,8] autonomous and programmed self-assembly of functional DNA nanostructures,[9] and DNA computing circuits.[10] For example, hybridization chain reaction (HCR), in which two metastable DNA hairpins coexist and assemble into polymeric nanowires through TM-SDR upon exposure to an initiator,[11] provides a general principle to isothermal amplification detection of various biorelated analytes,[12,13] cancer imaging and therapy,[14] and in situ multiplexed mapping of mRNAs.[15−17] In particular, nucleic acid hairpin structures might act as catalytic energetic traps that may be activated by an initiator to yield a variety of complex DNA nanostructures and nanomachines through a free-energy-driven isothermal autonomous catalytic hairpin assembly (CHA) process.[18] On the basis of the advantages of continuous signal turnover capability, inherent modularity, and easy scale-up, CHA has been developed for sensitive detection of DNA and small molecules,[19,20] and even for the construction of molecular keypad-lock systems.[21]

Up to now, the CHA products have generally been detected by fluorescent and colorimetric measurements. Alternatively, chemiluminescence (CL) that is induced by a chemical reaction without the requirement of an external excitation source has become a powerful tool for biochemical research with high sensitivity and simplified operation.[22] Especially, chemiluminescence resonance energy transfer (CRET) that occurs via nonradiative dipole−dipole energy transfer from a CL donor to a suitable acceptor when they are in close proximity can essentially minimize the nonspecific signals.[23] More importantly, coupling with a charge-coupled device (CCD) as a detector, CRET imaging is promising for versatile bioanalytical applications.[24,25]

Moreover, during the last few decades, DNA has emerged as building blocks for the construction of various nanostructures, which are typically relied on Watson−Crick base-pair hybridization between short DNA building blocks.[26−28] However, these conventional approaches often suffer from the intrinsic drawbacks of sophisticated sequence design, requirement of a large amount of DNA, limited compaction, and environment-sensitive disassembly. Therefore, a facile method for the assembly of densely compacted DNA nanostructures using only a few DNA strands, without reliance on Watson−Crick base-pairing, is still in high demand. Interestingly, it has been found that a tremendous amount of genomic double-stranded DNAs (dsDNAs) can be densely compacted into a liquid crystal-like structure in a highly ordered systematic manner that does not rely on Watson−Crick base-pairing.[29] Indeed, it has been reported that the synthetic short dsDNAs can also self-assemble into segregated structures through liquid crystallization without relying on Watson−Crick base-pairing when the concentrations are high enough to genomic DNA.[30] Recently, Tan's group developed a noncanonical self-assembly of hierarchical DNA nanoflowers through liquid crystallization of long and densely packed building blocks that were generated via rolling circle replication using only a low amount of two DNA strands, without reliance on Watson−Crick base-pairing.[31] More importantly, the targeting ligands (e.g., aptamer), functional moieties (e.g., antisense, interfering RNA, or other gene-regulation molecules), bioimaging agents (e.g., fluorophores), and drug loading sites (e.g., GC and CG base pairs for doxorubicin (Dox)) can be easily incorporated into the DNA nanostructures in a controlled manner. Therefore, the DNA nanostructures decorated with multifunctions have demonstrated promise as candidates for versatile applications in bioimaging, targeted drug delivery, and cancer therapeutics.

Herein, a DNA four-way junction (DNA-4WJ) is target-catalytically formed through cascade assembly of four DNA hairpins on the basis of DNA TM-SDR, in which G-quadruplex that can fold into HRP-mimicking DNAzyme in the presence of hemin is in a close proximity to fluorophore FAM, achieving ultrasensitive detection of microRNA taking advantage of isothermal target recycling amplification of CHA process and high sensitivity of CRET imaging assay. The typical problem of high background induced by excess hemin itself and unassembled hairpins is effectively overcome through absorbing them on magnetic graphene oxide (MGO) through π-stacking interactions and then removing via magnetic separation. Given the fabrication of DNA-4WJ in a cascaded manner, the proposed DNA-4WJ further extends to the construction of concatenated logic circuits composed of one YES gate and three AND gates with an automatic reset function by using four DNA hairpins as inputs. Moreover, after centrifugation, the formed DNA-4WJs serve as building units to self-assemble DNA nanohydrogels (~120 nm) driven by liquid crystallization and dense packing of DNA duplexes. By incorporating different functional elements, such as aptamers, bioimaging agents, and drug loading sites, into the building units, the synthesized aptamer-based DNA nanohydrogels are successfully applied in targeted drug delivery with high loading capacity and good biocompatibility.

In comparison with conventional methods, the major advantage of our strategy is being enzyme-free, in which the DNA-4WJs are target-catalytically formed through cascade assembly of four DNA hairpins without the requirement of any enzyme. Thus, the composition of our system is simple: it consists of only four DNA hairpins and one initiator. Other advantages are as follows. For biosensing, the target microRNA can be recycled automatically, resulting in the continuous generation of DNA-4WJs that bring HRP-mimicking DNAzyme and FAM in a close proximity to facilitate the sensitive CRET imaging assay. Moreover, the employment of MGO can easily remove unreacted hemin and DNA hairpin, which efficiently reduces the background and makes a great contribution to the improvement of detection sensitivity. For logic operations, unlike other reset biocomputing systems, the reset function of the current four-input concatenated logic circuits occurs spontaneously without addition of any external stimulus. For targeted drug delivery, the DNA nanohydrogels are self-assembled using DNA-4WJs as building units after centrifugation, which are driven by liquid crystallization and dense packaging of building units without relying on Watson−Crick base-pairing between DNA strands. Thus, it avoids the complicated design of DNA sequences that often occurs in conventional approaches to constructing DNA nanostructures. Therefore, our target-catalyzed DNA-4WJ holds great promise for wide applications in biosensing, biocomputing, biotechnology, and biomedicine.

DOI: 10.1021/acsami.5b07827
ACS Appl. Mater. Interfaces 2015, 7, 23310−23319

Scheme 1. Schematic Illustration of (A) Target MicroRNA-Catalyzed Formation of DNA-4WJ (Steps 1−5), Further Triggering the CRET Process in the Presence of Hemin/K^+ To form HRP-Mimicking DNAzymes That Catalyze the CL of Luminol/H_2O_2 and Transfer Energy to FAM (step 6), and (B) the Employment of MGO to Remove Unreacted DNA Hairpins and Hemin in Solution through π-Stacking Interactions to Reduce Background

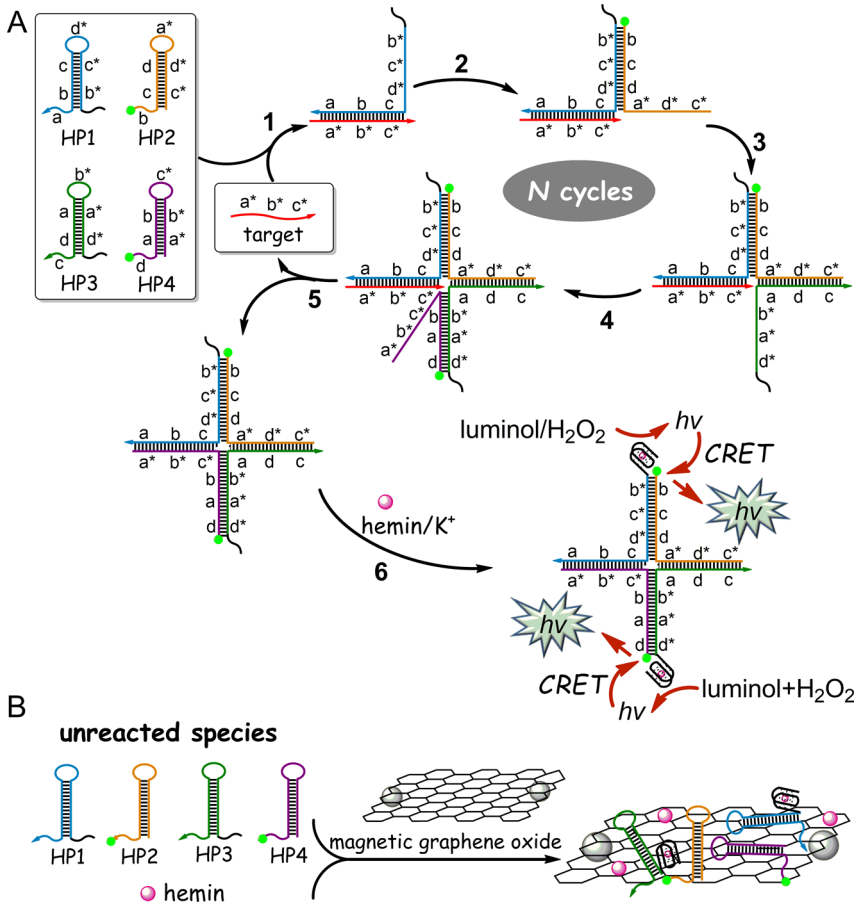

EXPERIMENTAL SECTION

Materials and Apparatus. The DNA hairpins and microRNAs used in this study were synthesized by Takara Biotechnology Co., Ltd. (Dalian, China) (see sequences listed in Table S1 and secondary structures presented in Figure S1), all of which were purified by high-performance liquid chromatography (HPLC). The Dulbecco's PBS (phosphate-buffered saline) and Cell Counting Kit-8 (CCK-8) kit were purchased from Sangon Biotech Co., Ltd. (Shanghai, China). Doxorubicin (Dox) was obtained from Aladdin Industrial, Inc. (Shanghai, China). The graphene oxide (GO) was ordered from XFNANO Co., Ltd. (Nanjing, China). Amino-modified magnetic particles (1−2 μm) and magnetic rack were purchased from BaseLine ChromTech Research Centre (Tianjin, China). All regents were of analytical grade, which were used as received unless otherwise stated. Double-distilled deionized water was used in all experiments.

Scanning electron microscopy (SEM) images were recorded with a JSM-6700F instrument (JEOL, Japan). CRET imaging was performed on an EC3 imaging system with a thermoelectrically cooled CCD camera (UVP, U.S.A.). The native polyacrylamide gel electrophoresis (PAGE) was carried out using a Beijing Liuyi WD-9413B gel imaging system (Beijing, China). The particle size of the DNA nanohydrogels was measured using a S3500 Microtrac particle size analyzer (Microtrac, Inc., U.S.A.). Fluorescent images were collected on a Leica TCS SP8 confocal laser scanning microscope (Leica, Germany). The UV−vis measurements were carried out on a Cary 50 UV−vis spectrometer (Varian, U.S.A.). All measurements were carried out at room temperature unless stated otherwise.

Native Polyacrylamide Gel Electrophoresis. The target-catalytic formation of DNA-4WJ was examined by 15% acrylamide gel (containing 29/1 acrylamide/bis(acrylamide) (w/w)) in 1× Tris−acetate ethylenediaminetetraacetate (TAE). Before addition into the gel for electrophoresis, the DNA samples were soaked with 1× loading buffer, followed by running at 170 V for 5 min and 110 V for 30 min at room temperature. After that, the gels were stained with diluted SYBR Green I solution for 30 min, then imaged under UV irradiation, and finally photographed by Liuyi WD-9413B gel imaging system (Beijing, China).

Preparation of MGO. GO was conjugated with magnetic particles according to our reported methods.[32] First, the carboxyl groups on GO were activated by mixing 600 μL of GO suspension (1 mg/mL) with 600 μL of 1-ethyl-3-(3-dimethyllaminopropyl)carbodiimide (EDC) (0.1 M) and 300 μL of *N*-hydroxysuccinimide (NHS) (0.1 M) in imidazole-HCl buffer (0.1 M, pH 6.8) and reacted at 37 °C for 1 h. Then, 300 μL of amino-modified magnetic particles (10 mg/mL) were added to the activated GO, followed by incubation at 37 °C overnight. Finally, the resultant MGO conjugates were washed with PBS (0.01 M, pH 7.4) through magnetic separation and resuspended in the same PBS solution before being used in the assay.

Target-Catalytic Formation of DNA-4WJ for CRET Imaging of MicroRNA. The DNA hairpins (HP1, HP2, HP3, and HP4) were respectively annealed (heat at 95 °C for 5 min, gradually cool to 25 °C at 1 °C/min, and stand at 25 °C for 1 h at least) in TE buffer (10 mM Tris-HCl, 1 mM EDTA-2Na, pH 8.0) supplemented with 12.5 mM $MgCl_2$ before use, ensuring the desirable secondary structures. Then, the annealed hairpins of HP4, HP3, HP2, and HP1 (1 μM for each species) were combined in that order, followed by the introduction of target miR-let-7a with different concentrations. After reaction at room temperature for 2 h, the solution of hemin (1 μM) was added and

DOI: 10.1021/acsami.5b07827
ACS Appl. Mater. Interfaces 2015, 7, 23310−23319

incubated at room temperature for 30 min, followed by introduction of the as-prepared MGO, allowing for reaction at room temperature for another 30 min. After magnetic separation, the supernatant containing the products of DNA-4WJs was transferred to a well of a 96-well plate. The CRET imaging was performed after introducing luminol (0.01 M) and H_2O_2 (0.3 M). The CRET signals were analyzed using the software equipped with the CL imager. The control experiments were carried out according to the same procedures, expect that no MGO was added into the system to capture the unreacted species (Scheme S1), or HP2 and HP4 without the modification of FAM were used to fabricate the DNA-4WJ (Scheme S2).

Four-Input Concatenated Logic Operation. The initial state of the concatenated logic circuits was the strand of target microRNA (1 μM). The inputs (A, B, C, and D) (1 μM for each) with different combinations were introduced into the system. Corresponding volume of TE buffer was used as a substitute when the input was a "0". After reaction at room temperature for 2 h, the solution of hemin (1 μM) was added and incubated at room temperature for 30 min. The following procedures of magnetic separation by MGO and CRET imaging were carried out as mentioned earlier.

Preparation of DNA Nanohydrogels. DNA species of annealed HP1, HP2, HP3, and HP4 (1 μM for each) were mixed with target microRNA (0.1 μM). After reaction at room temperature for 2 h, the resultant products were washed with double-distilled deionized water by centrifugation at 10 000 rpm for 1 min three times. The precipitate was resuspended in 20 μL of double-distilled deionized water for characterization or 100 μL of Dulbecco's PBS for drug loading and targeted drug delivery experiments. For aptamer-based DNA nanohydrogels, the same procedure was used, expect that aptamer sgc8-incorporated HP1′ and HP3′ were used to form the DNA-4WJ.

Drug Loading into DNA Nanohydrogels. Dox (1 mM) was incubated with 100 μL of the as-synthesized sgc8-based DNA nanohydrogels at room temperature for 24 h, followed by centrifugation at 10 000 rpm for 15 min. Afterward, the precipitate of the Dox-loaded sgc8-DNA nanohydrogels was dispersed in 100 μL of Dulbecco's PBS. To determine Dox loading amount into the sgc8-DNA nanohydrogels, the free Dox in supernatant was transferred to a quartz cuvette and quantified by UV−vis measurement at the absorbance of 480 nm. The amount of Dox loaded in sgc8-DNA nanohydrogels can be calculated by subtracting Dox amount in supernatant from total Dox amount.

Targeted Drug Delivery. The cytotoxicities of sgc8-DNA nanohydrogels, free Dox, and Dox-loaded sgc8-DNA nanohydrogels for target CCRF-CEM cells and control Ramos cells were evaluated using CCK-8 assay. Cell viability was determined according to the manufacturer's instructions.

RESULTS AND DISCUSSION

Target-Catalyzed Formation of DNA-4WJ for CRET Imaging of MicroRNA. As a class of endogenous and noncoding small RNA molecules, microRNAs play a key role in gene regulation. Thus, the development of rapid, sensitive, and quantitative methods for microRNA detection is imperative. Herein, we have developed a target-catalyzed and enzyme-free strategy for the formation of DNA-4WJs based on TM-SDR through assembly and disassembly pathways, which is further applied to sensitive and specific CRET imaging of microRNA. The principle is illustrated in Scheme 1A. In this study, microRNA-let-7a (miR-let-7a) is used as a proof-of-concept microRNA target. The complementary relationships between the segments of hairpins (HP1, HP2, HP3, and HP4) are specified. Each hairpin probe is rationally designed with a stem of 12 base pairs and a sticky end of 6 nucleotides at the 3′-end. In the absence of target microRNA, the hairpins can metastably coexist and are kinetically impeded from cross-opening. Otherwise, upon the introduction of target microRNA, an assembly reaction occurs when a* segment on target nucleates at the exposed toehold a of HP1, thus initiating a branch migration (that is, TM-SDR) to open HP1 with the formation of an intermediate target·HP1 (Scheme 1A, step 1). Then, the toehold of HP2 can hybridize to the newly exposed b* of HP1, thus again initiating a TM-SDR to open the HP2 and form a target·HP1·HP2 hybrid (Scheme 1A, step 2). Analogously, the newly accessible domains of HP2 serve as initiator to open HP3 to generate the assembly of target·HP1·HP2·HP3 (Scheme 1A, step 3), which further initiates the opening of HP4 to form the target·HP1·HP2·HP3·HP4 complex (Scheme 1A, step 4). Given the inherent unstability of the resultant complex, a spontaneous disassembly reaction occurs when a single-stranded domain (a*−b*−c*) of HP4 initiates a branch migration that displaces the target from the complex, thus forming a DNA four-arm junction (DNA-4WJ) and releasing the target to catalyze the next assembly−disassembly circle (Scheme 1A, step 5). As a result, a cascade of self-assembly steps can be catalyzed by target microRNA, and each assembly circle is terminated by a disassembly step in which HP4 displaces the target microRNA from the branched complex to form a DNA-4WJ. The reaction pathways are confirmed by native polyacrylamide gel electrophoresis (PAGE) (Figure S2).

In our strategy, HP1 and HP3 are modified with G-quadruplex fragments at the 5′-end, while HP2 and HP4 are labeled with fluorophore FAM at the 3′-end. Therefore, for the formed DNA-4WJ, upon incubation with hemin/K^+, HRP-mimicking DNAzymes are formed to catalyze the CL generation through the oxidation of luminol by H_2O_2, which further stimulates the CRET process to FAM due to the close proximity of DNAzyme units to FAM (Scheme 1A, step 6). The CRET signal is proportional to the concentration of target microRNA.

Although hemin/G-quadruplex HRP-mimicking DNAzymes could catalyze the CRET system with high catalytic efficiency, it has been reported that hemin itself has inherently catalytic ability toward the luminol/H_2O_2 CL system.[33,34] Thus, the unintercalated hemin can induce high background that would affect the detection sensitivity. Furthermore, the unreacted DNA species may also affect the detection system. For example, the G-rich sequences in additional HP1 and HP3 would integrate into G-quadruplex structure in the presence of hemin/K^+, leading to a negative signal that is not generated by target microRNA. In addition, in homogeneous reaction solution the unassembled FAM-labeled HP2 and HP4 can unavoidably induce a random CRET process (Scheme S1). To address these problems, as illustrated in Scheme 1B, magnetic graphene oxide (MGO) is introduced to the system to absorb the excess free hemin and unreacted DNA hairpins on graphene oxide (GO) surface through $\pi-\pi$ stacking interactions between hemin or single-stranded DNA (ssDNA) and GO.[35] In this study, MGO conjugates are readily fabricated through covalent reaction between aminos on magnetic particles and carboxyls on GO, which is characterized by SEM (Figure S3). As a result, the unreacted hemin and DNA hairpins can be easily removed from the solution through magnetic separation, which can not only simplify the operations without any DNA conjugation procedure but also improve the detection sensitivity by reducing the background.

To investigate the role of MGO in the system, a control experiment without MGO is carried out (Scheme S1). From Figure 1, in the absence of MGO, the homogeneous system suffers from random CRET signal and high background induced by free hairpins and hemin, which make it difficult

DOI: 10.1021/acsami.5b07827
ACS Appl. Mater. Interfaces 2015, 7, 23310−23319

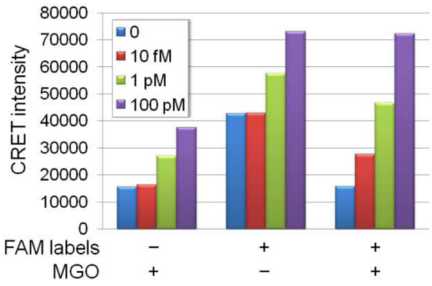

Figure 1. Comparison of the CRET intensities induced by different modes for the detection of miR-let-7a at the concentrations of 0, 10 fM, 1 pM, and 100 pM. The principle of each mode is illustrated in Scheme 1 (FAM labels, +; MGO, +), Scheme S1 (FAM labels, +; MGO, −), and Scheme S2 (FAM labels, −; MGO, +), respectively.

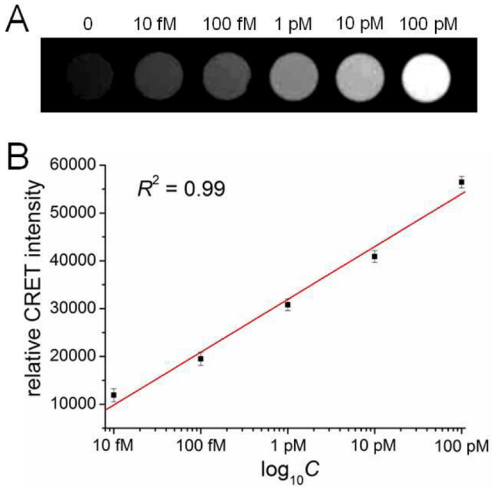

Figure 2. (A) CRET images and (B) corresponding calibration curve of the target-catalyzed DNA-4WJs for the detection of miR-let-7a using MGO to reduce background.

to discriminate the signal generated by 10 fM miR-let-7a against the background. However, as in the operation of Scheme 1 using MGO, after magnetic separation to remove the unreacted species, the resultant supernatant containing the target-catalyzed DNA-4WJs brings HRP-mimicking DNAzyme and FAM into close proximity and induces a CRET process upon the addition of luminol/H_2O_2. The CRET signals generated by 0 and 10 fM miR-let-7a can be easily distinguished from each other, promising high sensitivity for microRNA detection.

In the proposed CRET system, FAM acts as both acceptor and enhancer of the HRP-mimicking DNAzyme-catalyzed luminol/H_2O_2 CL system.[32] To confirm the effectiveness of the CRET system, instead of FAM modification, HP2 and HP4 with no labels (HP2′ and HP4′) are used to form the DNA-4WJs, following by CRET imaging assay after magnetic separation (Scheme S2). For this mode, although the background induced by luminol/H_2O_2 in the absence of target microRNA is significantly reduced through the employment of MGO to remove unreacted hairpins and hemin, for the detection of miR-let-7a at the same concentration, the CL signals generated by the target-catalyzed DNA-4WJs with only HRP-mimicking DNAzyme functionalization are greatly lower than that obtained by Scheme 1 (Figure 1), indicating the enhancing role of the acceptor FAM in this CRET system. Therefore, in this strategy, both MGO and FAM play important roles in improving the detection sensitivity.

Sensitivity and Specificity for CRET Imaging of Target MicroRNA. The sensitivity and dynamic range of the proposed DNA-4WJ for CRET imaging assay of microRNA are investigated with different concentrations of miRNA-let-7a. The visual images for qualitative analysis are displayed in Figure 2A. In the absence of miRNA-let-7a, no significant CRET signal is observed. When the concentration of miRNA-let-7a reaches 10 fM, the luminescence brightness can be easily distinguished with the blank and intensified with increasing miR-let-7a concentrations in the range from 100 fM to 100 pM. For quantitative analysis, the CRET intensities of the spots are collected using analysis software that is equipped with the CL imager. The corresponding calibration curve shows that the relative CRET intensities are linearly proportional to the logarithm of miR-let-7a concentrations in the range from 10 fM to 100 pM with a detection limit of 6.9 fM (3σ) and a determination coefficient (R^2) of 0.99 (Figure 2B). The ultrahigh sensitivity can be attributed to the automatic recycling of target microRNA to continuously generate DNA-4WJs that bring HRP-mimicking DNAzyme and FAM in close proximity to facilitate the sensitive CRET reaction, and also to the employment of MGO to efficiently reduce background.

The specificity of the proposed strategy for microRNA detection is further evaluated by monitoring the CRET signal yielded by different targets, including miR-let-7a, miR-let-7b, miR-let-7c, and miR-122. Only miR-let-7a produces a bright CRET signal, whereas all other controls at the same concentration hardly observe obvious intensity change against the blank sample (Figure S4). Therefore, only the target microRNA can initiate the TM-SDR to generate DNA-4WJs for CRET imaging, indicating the excellent selectivity of our assay.

Concatenated Logic Operations. The creation of DNA devices, especially Boolean logic gates, is a crucial requirement in the quest to build molecular-scale computers and is very essential for biological studies.[36,37] However, most of the logic operations are focused on the basic logic functions, such as AND, OR, or INHIBIT. Thus, the connection of biological logic gates into a multilevel circuit poses significant challenges. Given the fabrication of DNA-4WJ in a cascaded manner, it can be considered as a four-input concatenated logic gate composed of one YES gate and three AND gates, which are operated by stepwise treating of the network with different hairpins as inputs (A, B, C, and D) and the output of one gate as an input for a downstream gate (Scheme 2). The inputs are considered as 1 when they are present and 0 otherwise. For the outputs, the CRET signal generated by the supernatant containing the DNA-4WJ is defined as 1 ("true" output) or as 0 ("false" output) if the solution is without DNA-4WJ to generate a weak CRET signal that is below a threshold value. More importantly, the developed concatenated logic circuits can be automatically reset to the initial state upon the formation of DNA-4WJ. Unlike other reset biocomputing systems, the current reset function occurs spontaneously without addition of any external stimulus.

The corresponding CRET intensities obtained by different combinations of the four inputs are shown in Figure 3A. Accordingly, the output reads "1" only if all of the four inputs A, B, C, and D are present (1, 1, 1, 1) due to the formation of DNA-4WJ to yield a high CRET intensity. However, for other input combinations, because the products with single-stranded segments can be magnetically removed by MGO through π-stacking interactions between ssDNA and GO, no obvious

DOI: 10.1021/acsami.5b07827
ACS Appl. Mater. Interfaces 2015, 7, 23310−23319

Scheme 2. Schematic Illustration of the Four-Input Concatenated Logic Gates of YES−AND−AND−AND upon Activation by Inputs A, B, C, and D through TM-SDR

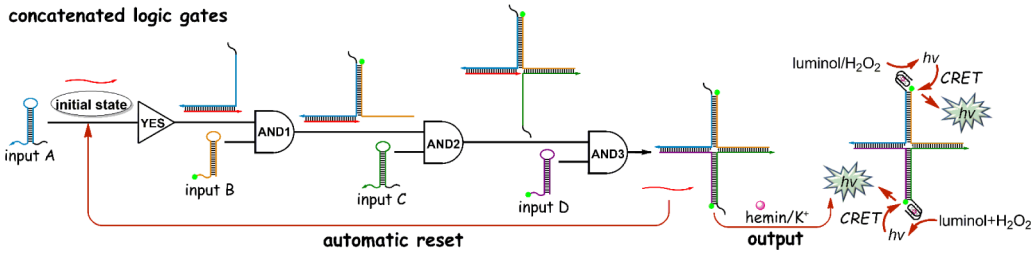

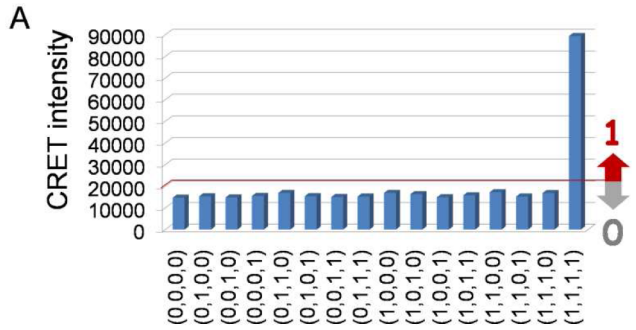

B

INPUT A	B	C	D	PRODUCTS	OUTPUT
0	0	0	0		0
0	1	0	0		0
0	0	1	0		0
0	0	0	1	unreacted HPs and microRNA, hemin/K+ MGO	0
0	1	1	0		0
0	1	0	1		0
0	0	1	1		0
0	1	1	1		0
1	0	0	0		0
1	0	1	0		0
1	0	0	1	hemin/K+ MGO	0
1	0	1	1		0
1	1	0	0		0
1	1	0	1	hemin/K+ MGO	0
1	1	1	0	hemin/K+ MGO	0
1	1	1	1	luminol/H2O2 hv CRET, hemin/K+ MGO, supernatant, hv CRET luminol+H2O2	1

Figure 3. (A) CRET intensities and (B) truth table of the four-input concatenated logic gates. The concentration of each component is 1 μM. The threshold CRET value of 20 000 is indicated by the red line in (A).

CRET signal of the supernatant is observed with a threshold value of 20 000 ("0" output). Therefore, the situations satisfy the operation of a concatenated YES−AND−AND−AND logic gate. The truth table is presented in Figure 3B.

The construction of four-input concatenated logic circuits using the DNA-4WJ architecture shows the feasible applications of the proposed strategies in not only the biosensing field but also molecular computation. In addition, the development of complex artificial biochemical networks that are able to perform basic computational operations is a key factor to develop diagnostic and therapeutic molecular devices. Therefore, our fabricated concatenated logic circuits may make a contribution to the advancement of molecular computation and DNA nanotechnology and also hold great potential in biological or medical applications.

Self-Assembly of DNA Nanohydrogels and Their Application in Targeted Drug Delivery. Interestingly, it is found that, after centrifugation of the resultant DNA-4WJs that are triggered by 0.1 μM target microRNA (0.1 equiv), DNA nanohydrogels are self-assembled through liquid crystallization and dense packing of DNA duplexes using DNA-4WJs as building units. The morphology and average particle size of the DNA nanohydrogels are characterized by scanning electron microscopy (SEM) and dynamic light scattering (DLS). No assembled product is observed in the absence of target microRNA (Figure 4A). In contrast, DNA nanohydrogels with monodispersity, well-defined spherical structures, and uniform size can be found upon the addition of target microRNA into the system after centrifugation (Figure 4B). DLS results reveal that the average radius of the assembled DNA nanohydrogels is 123 ± 14 nm (Figure 4C), which is consistent with the SEM data. In addition, only a small peak corresponding to a single DNA-4WJ unit is observed in DLS, indicating the highly efficient self-assembly of building units through centrifugation. It should be noted that in our strategy the DNA nanohydrogels are self-assembled using DNA-4WJs as building units through centrifugation, which are driven by liquid crystallization and dense packaging of DNA-4WJs. Thus, the concentration of building units and centrifugation are important for dense packaging of DNA-4WJs to be liquid crystalline. In our experiments, the DNA-4WJs with a high concentration of 0.25 μM were treated with centrifugation at 10 000 rmp for 1 min three times to ensure the formation DNA nanohydrogels.

The stability of the aptamer-functionalized DNA nanohydrogels is evaluated by treating them with human serum (10% diluted) at 37 °C for 24 h. The SEM observation verifies that the resultant DNA nanohydrogels still have spherical structure (Figure S5). This good stability can be attributed to the high density of DNA packed in each nanohydrogel, which efficiently prevents denaturation or dissociation, such as the cleavage of nuclease. Thus, our fabricated aptamer-based DNA nanohydrogels hold great promise for biomedical applications under complicated biological situations.

Taking advantage of the proposed strategy, the DNA nanohydrogels can be readily synthesized using only five DNAs based on liquid crystallization and dense packing from DNA duplexes. Thus, our approach is simple, avoids the involvement of complicated procedures (e.g., hybridization, enzymatic ligation, or photopolymerization)[38,39] and is useful

DOI: 10.1021/acsami.5b07827
ACS Appl. Mater. Interfaces 2015, 7, 23310−23319

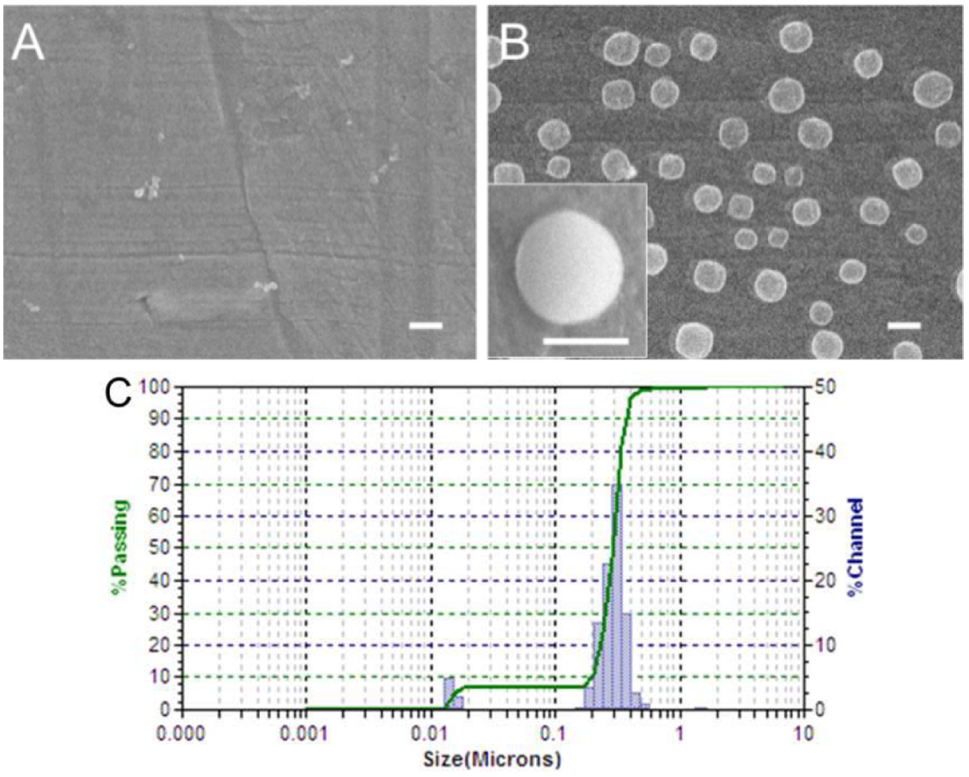

Figure 4. SEM images of (A) the products in the absence of target microRNA and (B) the DNA nanohydrogels in the presence of target. The concentration of each hairpin is 1 μM (1 equiv), while it is 0.1 μM (0.1 equiv) for target microRNA. (C) Size distribution of the DNA hydrogel nanoparticles obtained in (B) by DLS measurement. Scale bar = 100 nm.

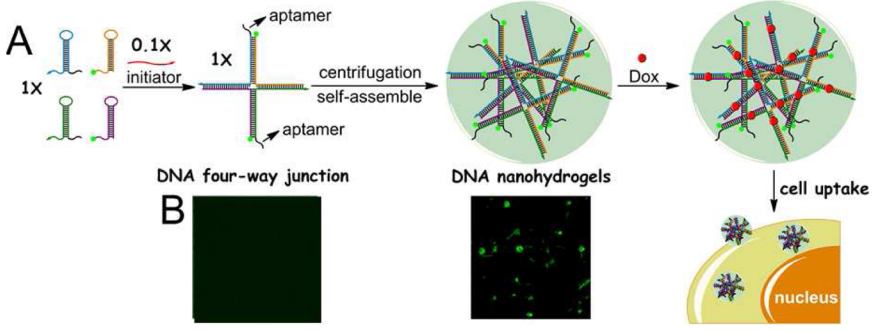

Figure 5. (A) Schematic illustration of self-assembly of aptamer-based DNA nanohydrogels using DNA-4WJ as a building unit that are further used as Dox carriers for targeted drug delivery in cancer cells. (B) DNA-4WJs and the aptamer-incorporated DNA nanohydrogels are characterized by fluorescence microscopy imaging. Scale bar = 1 μm.

to shorten the preparation time and reduce the damage to DNAs. Moreover, because there are a large number of packed DNA base pairs, the DNA nanohydrogels spatially facilitate for cargo loading, especially for chemotherapeutic drugs such as doxorubicin (Dox) that can preferentially intercalate into double-stranded GC or CG base pairs. To achieve targeted drug delivery, aptamer sgc8 that targets CCRF-CEM cells (T-cell, human acute lymphoblastic leukemia cell line) but not Ramos cells (B-cell, human Burkitt's lymphoma cell line) is conjugated into the 5′-end of HP1 and HP3 (HP1′ and HP3′), which are used to create a building unit of DNA-4WJ and further self-assemble into DNA nanohydrogels after centrifugation (Figure 5A). The resultant aptamer-functionalized DNA nanohydrogels are verified by fluorescence microscopy imaging (Figure 5B), which holds great promise for fluorescence bioimaging.

Theoretically, each target-catalyzed DNA-4WJ unit can provide ~30 specific loading sites for Dox. To load Dox into the sgc8-based DNA nanohydrogels, excess Dox is added to allow saturation of drug loading. After centrifugation, the unintercalated Dox in supernatant is isolated and its amount is determined by UV−vis measurement. It is calculated that 1 nM sgc8-based DNA nanohydrogels can load ~3 μM Dox, indicating a high drug loading capacity of the DNA nanohydrogels. To study selective transport of anticancer drug into target cancer cells, confocal microscopy imaging is carried out by incubating target CCRF-CEM cells and control Ramos cells with Dox-loaded sgc8-DNA nanohydrogels for 2 h to visually demonstrate the intracellular uptake and distribution of Dox delivered via the aptamer-based DNA nanohydrogels. As expected, the fluorescence of Dox is restored in CCRF-CEM cells by releasing from sgc8-DNA nanohydrogels (Figure 6A)

DOI: 10.1021/acsami.5b07827
ACS Appl. Mater. Interfaces 2015, 7, 23310−23319

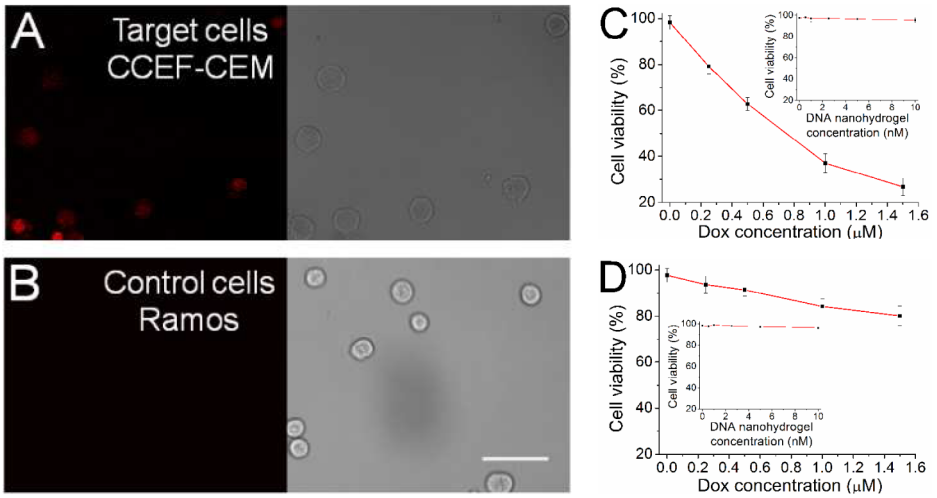

Figure 6. Confocal fluorescence images and cytotoxicity studies of Dox delivered via sgc8-based DNA nanohydrogels in target CCRF-CEM cells (A and C) and nontarget Ramos cells (B and D). Insets of (C and D) show the CCK-8 assay results obtained by treating CCRF-CEM cells and Ramos cells with the sgc8-based DNA nanohydrogels to verify the biocompatibility. Scale bar = 20 μm.

but not in Ramos cells (Figure 6B), indicating the selective delivery of Dox mediated by aptamer-based DNA nanohydrogels.

For further targeted drug delivery studies, target CCRF-CEM cells and nontarget Ramos cells are treated with free Dox and Dox-loaded sgc8-DNA nanohydrogels, respectively. The in vitro cytotoxicity is evaluated by CCK-8 assay. From Figure S6, free Dox exhibits a dose-dependent cytotoxicity behavior in either CCRF-CEM cells or Ramos cells, indicating nonselective cytotoxicity of free Dox in cancer cells. However, for Dox-loaded sgc8-DNA nanohydrogels, an efficient and dose-dependent cytotoxicity is only observed in target CCRF-CEM cells (Figure 6C) but not in nontarget Ramos cells (Figure 6D). In addition, in CCRF-CEM cells, Dox delivered by sgc8-DNA nanohydrogels induces only slightly less inhibition of cell proliferation than free Dox. The selective cytotoxicity of Dox delivered by aptamer-based DNA nanohydrogels demonstrates its capability of targeted drug delivery. Moreover, the biocompatibility of the sgc8-DNA nanohydrogels without loading Dox is also verified by CCK-8 assay (inset of Figure 6C and 6D). The results show that even the concentration of building units at 10 nM, a negligible inhibition of proliferation in CCRF-CEM cells is exhibited with the cell viability more than 95%. Therefore, the Dox-loaded and aptamer-functionalized DNA nanohydrogels demonstrate the advantages of high loading capacity, selective cytotoxicity, and excellent biocompatibility, promising its application in targeted drug delivery and potential cancer therapy.

CONCLUSION

In summary, we have developed a fascinating building unit of DNA-4WJ based on targeted-catalytic formation and toehold-mediated strand displacement, which is versatilely applied in biosensing, logic operations, and self-assembly of DNA nanohydrogels for targeted drug delivery. By rationally embedding HRP-mimicking DNAzymes and FAM into DNA-4WJs in a close proximity and employing MGO to reduce background, the signals of the formed DNA-4WJs can be sensitively read out by a CCD to perform CRET imaging, achieving enzyme-free and cascaded amplification detection of miR-let-7a with a detection limit of 6.9 fM and excellent specificity. The DNA-4WJ architecture is further utilized to construct four-input concatenated logic circuits that can be easily reset and cycled automatically. More importantly, without relying on Watson−Crick base-pairing, the target-catalyzed DNA-4WJs are employed as building units to self-assemble DNA nanohydrogels through centrifugation that are driven by liquid crystallization and dense packing of DNA duplexes, exhibiting monodispersity and good biocompatibility. By incorporating functional elements, such as aptamers, drug loading sites, and fluorescent bioimaging agents, into the building units, the DNA nanohydrogels are used as effective drug nanocarriers with high payload capacity for specific recognition and selective cytotoxicity of target cancer cells. Therefore, our target-catalyzed DNA branched junctions provide wide potential applications in biochemical fields, including biosensing, biocomputing, biotechnology, and biomedicine.

ASSOCIATED CONTENT

Supporting Information

The Supporting Information is available free of charge on the ACS Publications website at DOI: 10.1021/acsami.5b07827.

Oligonucleotide sequences, native polyacrylamide gel electrophoresis (PAGE), control experiments, characterization of MGO conjugates, specificity of the target-catalyzed DNA-4WJ for CRET imaging of miR-let-7a, stability of the aptamer-based DNA nanohydrogels, cytotoxicity study of free Dox (PDF)

AUTHOR INFORMATION

Corresponding Author

*E-mail: sdqdbs@126.com.

Notes

The authors declare no competing financial interest.

ACKNOWLEDGMENTS

This work was supported by the National Science Foundation of China (21375056 and 21535002), the Program for New Century Excellent Talents in University of Ministry of Education of China (NCET-12-1024), and the Open Funds

DOI: 10.1021/acsami.5b07827
ACS Appl. Mater. Interfaces 2015, 7, 23310−23319

of the Shandong Province Key Laboratory of Detection Technology for Tumor Markers (KLDTTM2015-1).

REFERENCES

(1) Wang, F.; Lu, C.-H; Willner, I. From Cascaded Catalytic Nucleic Acids to Enzyme-DNA Nanostructures: Controlling Reactivity, Sensing, Logic Operations, and Assembly of Complex Structures. *Chem. Rev.* **2014**, *114*, 2881−2941.
(2) Lu, C.-H.; Willner, B.; Willner, I. DNA Nanotechnology: From Sensing and DNA Machines to Drug-Delivery Systems. *ACS Nano* **2013**, *7*, 8320−8332.
(3) Wilner, O. I.; Willner, I. Functionalized DNA Nanostructures. *Chem. Rev.* **2012**, *112*, 2528−2556.
(4) Peng, L.; Wu, C. S.; You, M.; Han, D.; Chen, Y.; Fu, T.; Ye, M.; Tan, W. Engineering and Applications of DNA-Grafted Polymer Materials. *Chem. Sci.* **2013**, *4*, 1928−1938.
(5) Wang, F.; Liu, X.; Willner, I. DNA Switches: From Principles to Applications. *Angew. Chem., Int. Ed.* **2015**, *54*, 1098−1129.
(6) Zhang, Z.; Cheng, Q.; Feng, P. Selective Removal of DNA-Labeled Nanoparticles from Planar Substrates by DNA Displacement Reactions. *Angew. Chem., Int. Ed.* **2009**, *48*, 118−122.
(7) Huang, F.; You, M.; Han, D.; Xiong, X.; Liang, H.; Tan, W. DNA Branch Migration Reactions Through Photocontrollable Toehold Formation. *J. Am. Chem. Soc.* **2013**, *135*, 7967−7973.
(8) Xuan, F.; Hsing, I.-M. Triggering Hairpin-Free Chain-Branching Growth of Fluorescent DNA Dendrimers for Nonlinear Hybridization Chain Reaction. *J. Am. Chem. Soc.* **2014**, *136*, 9810−9813.
(9) Zhang, D. Y.; Hariadi, R. F.; Choi, H. M. T.; Winfree, E. Integrating DNA Strand-Displacement Circuitry with DNA Tile Self-Assembly. *Nat. Commun.* **2013**, *4*, 1965.
(10) Ruiz, I. M.; Arbona, J.-M.; Lad, A.; Mendoza, O.; Aimé, J.-P.; Elezgaray, J. Connecting Localized DNA Strand Displacement Reactions. *Nanoscale* **2015**, *7*, 12970−12978.
(11) Dirks, R. M.; Pierce, N. A. Triggered Amplification by Hybridization Chain Reaction. *Proc. Natl. Acad. Sci. U. S. A.* **2004**, *101*, 15275−15278.
(12) Huang, J.; Wu, Y.; Chen, Y.; Zhu, Z.; Yang, X.; Yang, C. J.; Wang, K.; Tan, W. Pyrene-Excimer Probes Based on the Hybridization Chain Reaction for the Detection of Nucleic Acids in Complex Biological Fluids. *Angew. Chem., Int. Ed.* **2011**, *50*, 401−404.
(13) Bi, S.; Chen, M.; Jia, X.; Dong, Y.; Wang, Z. Hyperbranched Hybridization Chain Reaction for Triggered Signal Amplification and Concatenated Logic Circuits. *Angew. Chem., Int. Ed.* **2015**, *54*, 8144−8148.
(14) Zhu, G.; Zheng, J.; Song, E.; Donovan, M.; Zhang, K.; Liu, C.; Tan, W. Self-Assembled, Aptamer-Tethered DNA Nanotrains for Targeted Transport of Molecular Drugs in Cancer Theranostics. *Proc. Natl. Acad. Sci. U. S. A.* **2013**, *110*, 7998−8003.
(15) Choi, H. M. T.; Chang, J. Y.; Trinh, L. A.; Padilla, J. E.; Fraser, S. E.; Pierce, N. A. Programmable *In Situ* Amplification for Multiplexed Imaging of mRNA Expression. *Nat. Biotechnol.* **2010**, *28*, 1208−1212.
(16) Choi, H. M. T.; Beck, V. A.; Pierce, N. A. Next-Generation *In Situ* Hybridization Chain Reaction: Higher Gain, Lower Cost, Greater Durability. *ACS Nano* **2014**, *8*, 4284−4294.
(17) Wu, Z.; Liu, G.-Q.; Yang, X.-L.; Jiang, J.-H. Electrostatic Nucleic Acid Nanoassembly Enables Hybridization Chain Reaction in Living Cells for Ultrasensitive mRNA Imaging. *J. Am. Chem. Soc.* **2015**, *137*, 6829−6836.
(18) Yin, P.; Choi, H. M. T.; Calvert, C. R.; Pierce, N. A. Programming Biomolecular Self-Assembly Pathways. *Nature* **2008**, *451*, 318−322.
(19) Qing, Z.; He, X.; Huang, J.; Wang, K.; Zou, Z.; Qing, T.; Mao, Z.; Shi, H.; He, D. Target-Catalyzed Dynamic Assembly-Based Pyrene Excimer Switching for Enzyme-Free Nucleic Acid Amplified Detection. *Anal. Chem.* **2014**, *86*, 4934−4939.
(20) Chen, J.; Wen, J.; Yang, G.; Zhou, S. A Target-Induced Three-Way G-quadruplex Junction for 17β-estradiol Monitoring with a Naked-Eye Readout. *Chem. Commun.* **2015**, *51*, 12373−12376.
(21) Chen, J.; Zhou, S.; Wen, J. Concatenated Logic Circuits Based on a Three-Way DNA Junction: A Keypad-Lock Security System with Visible Readout and an Automatic Reset Function. *Angew. Chem.* **2015**, *127*, 456−460.
(22) Das, S.; Powe, A. M.; Baker, G. A.; Valle, B.; El-Zahab, B.; Sintim, H. O.; Lowry, M.; Fakayode, S. O.; McCarroll, M. E.; Patonay, G.; Li, M.; Strongin, R. M.; Geng, M. L.; Warner, I. M. Molecular Fluorescence, Phosphorescence, and Chemiluminescence Spectrometry. *Anal. Chem.* **2012**, *84*, 597−625.
(23) Freeman, R.; Girsh, J.; Willner, I. Nucleic Acid/Quantum Dots (QDs) Hybrid Systems for Optical and Photoelectrochemical Sensing. *ACS Appl. Mater. Interfaces* **2013**, *5*, 2815−2834.
(24) Bi, S.; Ji, B.; Zhang, Z.; Zhang, S. A Chemiluminescence Imaging Array for the Detection of Cancer Cells by Dual-Aptamer Recognition and Bio-Bar-Code Nanoprobe-Based Rolling Circle Amplification. *Chem. Commun.* **2013**, *49*, 3452−3454.
(25) Bi, S.; Zhang, Z.; Dong, Y.; Wang, Z. Chemiluminescence Resonance Energy Transfer Imaging on Magnetic Particles for Single-Nucleotide Polymorphism Detection Based on Ligation Chain Reaction. *Biosens. Bioelectron.* **2015**, *65*, 139−144.
(26) Li, J.; Zheng, C.; Cansiz, S.; Wu, C.; Xu, J.; Cui, C.; Liu, Y.; Hou, W.; Wang, Y.; Zhang, L.; Teng, I.; Yang, H.-H.; Tan, W. Self-assembly of DNA Nanohydrogels with Controllable Size and Stimuli-Responsive Property for Targeted Gene Regulation Therapy. *J. Am. Chem. Soc.* **2015**, *137*, 1412−1415.
(27) Xing, Y.; Cheng, E.; Yang, Y.; Chen, P.; Zhang, T.; Sun, Y.; Yang, Z.; Liu, D. Self-assembled DNA Hydrogels with Designable Thermal and Enzymatic Responsiveness. *Adv. Mater.* **2011**, *23*, 1117−1121.
(28) Meng, H.-M.; Zhang, X.; Lv, Y.; Zhao, Z.; Wang, N.-N.; Fu, T.; Fan, H.; Liang, H.; Qiu, L.; Zhu, G.; Tan, W. DNA Dendrimer: An Efficient Nanocarrier of Functional Nucleic Acids for Intracellular Molecular Sensing. *ACS Nano* **2014**, *8*, 6171−6181.
(29) Chow, M. H.; Yan, K. T. H.; Bennett, M. J.; Wong, J. T. Y. Birefringence and DNA Condensation of Liquid Crystalline Chromosomes. *Eukaryotic Cell* **2010**, *9*, 1577−1587.
(30) Zanchetta, G.; Nakata, M.; Buscaglia, M.; Bellini, T.; Clark, N. A. Phase Separation and Liquid Crystallization of Complementary Sequences in Mixtures of NanoDNA Oligomers. *Proc. Natl. Acad. Sci. U. S. A.* **2008**, *105*, 1111−1117.
(31) Zhu, G.; Hu, R.; Zhao, Z.; Chen, Z.; Zhang, X.; Tan, W. Noncanonical Self-Assembly of Multifunctional DNA Nanoflowers for Biomedical Applications. *J. Am. Chem. Soc.* **2013**, *135*, 16438−16445.
(32) Bi, S.; Chen, M.; Jia, X.; Dong, Y. A Hot-Spot-Active Magnetic Graphene Oxide Substrate for MicroRNA Detection Based on Cascaded Chemiluminescence Resonance Energy Transfer. *Nanoscale* **2015**, *7*, 3745−3753.
(33) Bi, S.; Zhang, J.; Zhang, S. Ultrasensitive and Selective DNA Detection Based on Nicking Endonuclease Assisted Signal Amplification and Its Application in Cancer Cell Detection. *Chem. Commun.* **2010**, *46*, 5509−5511.
(34) Guo, Y.; Deng, L.; Li, J.; Guo, S.; Wang, E.; Dong, S. Hemin-Graphene Hybrid Nanosheets with Intrinsic Peroxidase-like Activity for Label-free Colorimetric Detection of Single-Nucleotide Polymorphism. *ACS Nano* **2011**, *5*, 1282−1290.
(35) Lu, C.-H.; Li, J.; Lin, M.-H.; Wang, Y.-W.; Yang, H.-H.; Chen, X.; Chen, G.-N. A Graphene Platform for Sensing Biomolecules. *Angew. Chem., Int. Ed.* **2009**, *48*, 4785−4787.
(36) Guo, Y.; Wu, J.; Ju, H. Target-Driven DNA Association to Initiate Cyclic Assembly of Hairpins for Biosensing and Logic Gate Operation. *Chem. Sci.* **2015**, *6*, 4318−4323.
(37) He, K.; Li, Y.; Xiang, B.; Zhao, P.; Hu, Y.; Huang, Y.; Li, W.; Nie, Z.; Yao, S. A Universal Platform for Building Molecular Logic Circuits Based on a Reconfigurable Three-Dimensional DNA Nanostructure. *Chem. Sci.* **2015**, *6*, 3556−3564.
(38) Wu, C.; Han, D.; Chen, T.; Peng, L.; Zhu, G.; You, M.; Qiu, L.; Sefah, K.; Zhang, X.; Tan, W. Building a Multifunctional Aptamer-Based DNA Nanoassembly for Targeted Cancer Therapy. *J. Am. Chem. Soc.* **2013**, *135*, 18644−18650.

DOI: 10.1021/acsami.5b07827
ACS Appl. Mater. Interfaces 2015, 7, 23310−23319

(39) Bi, S.; Dong, Y.; Jia, X.; Chen, M.; Zhong, H.; Ji, B. Self-Assembled Multifunctional DNA Nanospheres for Biosensing and Drug Delivery into Specific Target Cells. *Nanoscale* **2015**, *7*, 7361−7367.

DOI: 10.1021/acsami.5b07827
ACS Appl. Mater. Interfaces 2015, 7, 23310−23319